ACSNANO
www.acsnano.org
ARTICLE

Highly Stable Near-Unity Photoluminescence Yield in Monolayer MoS_2 by Fluoropolymer Encapsulation and Superacid Treatment

Hyungjin Kim,[†,‡,∥] Der-Hsien Lien,[†,‡,∥] Matin Amani,[†,‡] Joel W. Ager,[‡,§] and Ali Javey*[,†,‡]

[†]Department of Electrical Engineering and Computer Sciences and [§]Department of Materials Science and Engineering, University of California, Berkeley, California 94720, United States

[‡]Materials Sciences Division, Lawrence Berkeley National Laboratory, Berkeley, California 94720, United States

Supporting Information

ABSTRACT: Recently, there has been considerable research interest in two-dimensional (2D) transition-metal dichalcogenides (TMDCs) for future optoelectronic applications. It has been shown that surface passivation with the organic nonoxidizing superacid bis(trifluoromethane)sulfonamide (TFSI) produces MoS_2 and WS_2 monolayers whose recombination is at the radiative limit, with a photoluminescence (PL) quantum yield (QY) of ~100%. While the surface passivation persists under ambient conditions, exposure to conditions such as water, solvents, and low pressure found in typical semiconductor processing degrades the PL QY. Here, an encapsulation/passivation approach is demonstrated that yields near-unity PL QY in MoS_2 and WS_2 monolayers which are highly stable against postprocessing. The approach consists of two simple steps: encapsulation of the monolayers with an amorphous fluoropolymer and a subsequent TFSI treatment. The TFSI molecules are able to diffuse through the encapsulation layer and passivate the defect states of the monolayers. Additionally, we demonstrate that the encapsulation layer can be patterned by lithography and is compatible with subsequent fabrication processes. Therefore, our work presents a feasible route for future fabrication of highly efficient optoelectronic devices based on TMDCs.

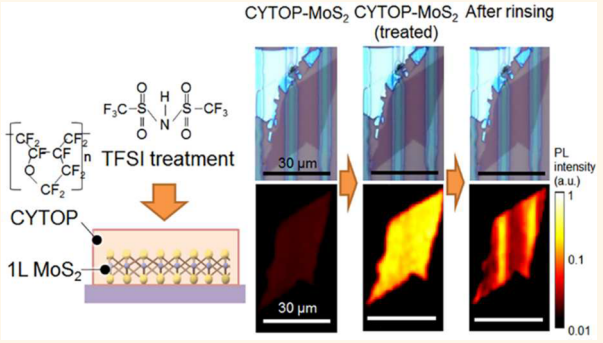

KEYWORDS: *2D materials, encapsulation, quantum yield, photoluminescence, stability*

Two-dimensional (2D) transition-metal dichalcogenides (TMDCs), such as MoS_2 and WSe_2, have a number of properties which make them promising for future optoelectronic devices.[1−5] TMDC monolayers have direct optical band gaps ranging from 0.8 to 2.0 eV[6,7] which can be tuned through electric field and strain.[8−10] In addition, these materials can readily be fabricated into van der Waals heterostructures without the need for lattice matching.[11,12] While these properties could enable the application of TMDCs for various optoelectronic devices, including lasers, photodetectors, and light-emitting diodes (LEDs),[13−15] numerous obstacles must still be overcome before they can be implemented in practical applications. One of the main constraints is the low photoluminescence (PL) quantum yield (QY) at room temperature for as-processed monolayers, which is reported to be in the range of 0.01−6%.[16] This is attributed to the defect states within TMDCs which contribute to nonradiative recombination and accordingly reduce the PL QY.[17−19] Among various strategies that have been tried to improve the QY of TMDCs,[20−22] chemical treatment by the nonoxidizing organic superacid, bis(trifluoromethane)sulfonamide (TFSI) has been shown to dramatically enhance the PL QY of exfoliated MoS_2 monolayers to near 100% at low injection levels, resulting in optoelectronically perfect monolayers.[23] The superacid treatment can effectively passivate the defect states in sulfur-based TMDCs, such as MoS_2 and WS_2, thus dramatically reducing the defect-mediated nonradiative recombination of carriers.[24]

While the achievement of surface passivated TMDCs is encouraging, the passivation does not persist during subsequent device fabrication and processing. For example, the enhancement in PL QY is easily removed after exposure to water and commonly used organic solvents including acetone. In this work, encapsulation of MoS_2 monolayers with CYTOP, which is an amorphous perfluorinated polymer with environmental stability and high optical transparency, is explored. This CYTOP-encapsulated TMDC monolayer is subsequently treated by

Received: April 11, 2017
Accepted: May 3, 2017
Published: May 3, 2017

DOI: 10.1021/acsnano.7b02521
ACS Nano 2017, 11, 5179−5185

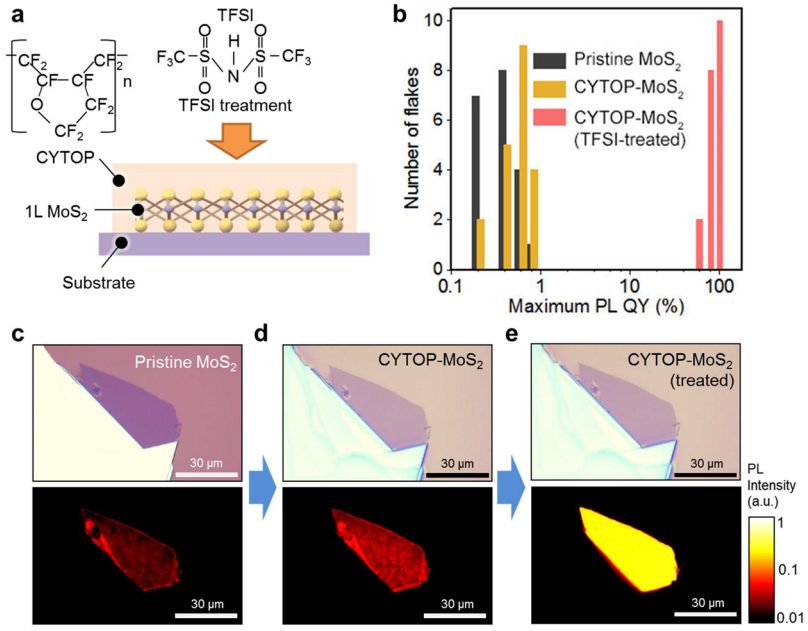

Figure 1. (a) Schematic of sample encapsulation/passivation scheme, showing a monolayer of MoS_2 coated by CYTOP and subsequently treated by TFSI. (b) Histogram showing the PL QY of 20 MoS_2 flakes measured at an incident laser power of 1×10^{-2} W cm^{-2} after exfoliation, coating by CYTOP, and treatment by TFSI. (c–e) PL images and corresponding optical micrographs of a MoS_2 monolayer (c) after exfoliation, (d) coating by CYTOP, and (e) treatment by TFSI; PL images are plotted on a common logarithmic scale.

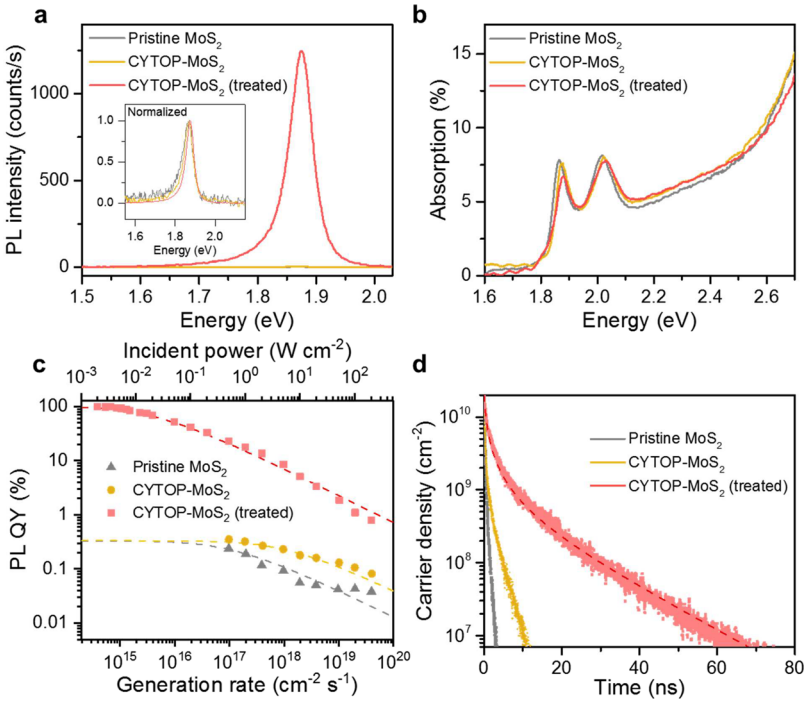

Figure 2. (a) PL spectra measured at an incident power of 2 W cm^{-2} for an as-exfoliated MoS_2 monolayer, after coating by CYTOP and after treatment by TFSI; inset shows normalized spectra. (b) Absorption spectra measured for an as-exfoliated MoS_2 monolayer, after coating by CYTOP and after treatment by TFSI. (c) PL QY as a function of incident laser power measured on an as-exfoliated MoS_2 monolayer, after coating by CYTOP and after treatment by TFSI. (d) Time-resolved PL decay measured on an as-exfoliated MoS_2 monolayer, after coating by CYTOP and after treatment by TFSI.

TFSI, resulting in the near-unity PL QY with excellent stability under subsequent processing. We show that the dramatically improved optoelectronic properties of the TMDC monolayer can be directly attributed to the TFSI diffusion through the encapsulating layer which effectively passivates the defect sites, suggesting that this technique can be employed generally for the development of monolayer optoelectronic devices with high efficiency.

RESULTS AND DISCUSSION

Figure 1a shows a schematic of the encapsulation/passivation scheme. First, a MoS_2 monolayer is encapsulated by CYTOP

DOI: 10.1021/acsnano.7b02521
ACS Nano 2017, 11, 5179–5185

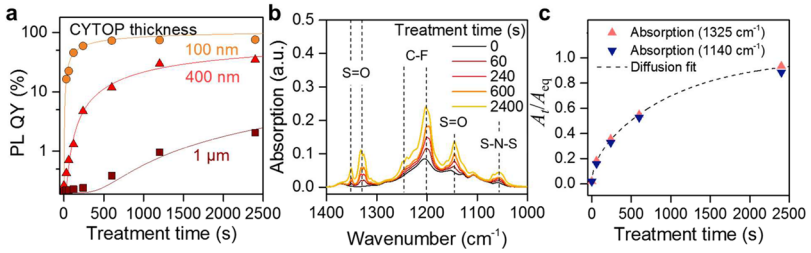

Figure 3. (a) PL QY as a function of treatment time for MoS_2 samples coated by 100 nm, 400 nm, and 1 μm thick CYTOP films. Solid lines result from the defect passivation model described by eqs 4 and 6. (b) Absorption spectra measured on a 100 nm CYTOP film coated on a KBr substrate as a function of TFSI treatment time. (c) IR absorption near 1325 and 1140 cm^{-1} of the TFSI diffused through 100 nm CYTOP film coated on a KBr substrate as a function of the TFSI treatment time. A_t and A_{eq} denote the absorption at time t and at equilibrium. Line is a fit to eq 5 with a TFSI diffusion coefficient of 1.1×10^{-14} cm^2 s^{-1}.

deposited by spin-coating followed by thermal annealing. Next, the encapsulated MoS_2 is immersed in a TFSI solution (see Methods for details). It should be noted that although the superacid treatment can also be applied to the other sulfur based TMDCs such as WS_2 as shown in Figure S1, we focus on the process and characterization of exfoliated MoS_2 monolayers, for the scope of this paper. The PL QY measured at a laser power below the onset of biexitonic recombination is used as a figure of merit. The optimal CYTOP thickness for maximizing the PL QY was found to be 60−200 nm when the TFSI concentration of the solution is 0.2 mg/mL. As shown in the histogram in Figure 1b, compared with the QY of untreated CYTOP-coated MoS_2 and the QY of as-exfoliated MoS_2 monolayers, the QY of CYTOP-coated MoS_2 monolayers after superacid treatment was consistently enhanced by over 2 orders of magnitude. Based on the optimized CYTOP and TFSI treatment for 20 samples, the QY of MoS_2 monolayers was within the range of 55% to near 100%.

Optical and PL images of pristine, untreated CYTOP-coated, and treated CYTOP-coated MoS_2 monolayer are shown in Figure 1c−e. In addition to the uniform enhancement of PL emission in the CYTOP-coated MoS_2 monolayer after superacid treatment, these images show that there were no significant visible changes in the surface by encapsulation or superacid treatment. In addition, the surface morphologies of MoS_2 monolayer after encapsulation and superacid treatment were characterized by atomic force microscopy (AFM) and showed no visible changes, as shown in Figure S2.

We performed detailed steady-state and transient PL measurements to characterize the optoelectronic properties of MoS_2 before and after treatment. PL spectra of MoS_2 monolayers measured at an incident power of 2 W cm^{-2} are shown in Figure 2a and indicate that the PL intensity was enhanced by over 2 orders of magnitude after superacid treatment. Furthermore, as shown in the inset of Figure 2a, we do not detect a measurable peak shift after both CYTOP encapsulation and TFSI treatment, with the only significant spectral change being the reduction in the low-energy tail after treatment. Additionally, using the quantitative absorption measurements with two different methods as described in previous studies,[23,24] we observed that CYTOP coating and the superacid treatment do not have significant effects on the light absorption in the range of 1.6−2.6 eV, as shown in Figure 2b. The pump-power behavior of the PL QY in MoS_2 monolayers was measured over a dynamic range of 6 orders of magnitude, as shown in Figure 2c. According to the previously reported recombination model,[23] the QY is given as

$$\mathrm{QY} = \frac{\tau_r^{-1}\langle N\rangle}{\tau_r^{-1}\langle N\rangle + B_{nr}n^2 + C_{bx}\langle N\rangle^2} \quad (1)$$

where τ_r is the radiative lifetime, $\langle N\rangle$ is the exciton concentration, B_{nr} is the defect-mediated nonradiative recombination rate, C_{bx} is the biexcitonic recombination rate, and n is the optically generated electron concentration, which is equal to the hole concentration for lightly doped semiconductors. For the untreated samples without and with CYTOP, both QY curves can be fit to the recombination models with the same value of $B_{nr} = 3 \times 10^6$ cm^2 s^{-1}, respectively. In the case of the treated CYTOP-coated samples where B_{nr} is negligible, the QY results fit the recombination model with a $C_{bx} = 0.3$ cm^2 s^{-1}, which is consistent with previous reports.[23] The PL QY of CYTOP-encapsulated MoS_2 monolayer after superacid treatment approaches 100% at a low pump intensity ($<5 \times 10^{-2}$ W cm^{-2}). From the coefficients extracted in the recombination model, we found that the encapsulation of MoS_2 with CYTOP affects the biexcitonic recombination rate (C_{bx}) without changing B_{nr}, while the superacid treatment suppresses the defect-mediated nonradiative recombination (B_{nr}) without affecting C_{bx}. The reduction of C_{bx} results in a slight increase of the PL at high injection levels. The C_{bx} reduction can most likely be attributed to the change of the dielectric surroundings from air/MoS_2/substrate to CYTOP/MoS_2/substrate where CYTOP has a refractive index of 1.34. C_{bx} is expected to vary with encapsulation layers because the exciton−exciton interaction is strongly coupled with dielectric environments due to screening effects.

The impact of superacid treatment on the CYTOP-encapsulated MoS_2 monolayers was further evaluated *via* the carrier recombination dynamics measured from time-resolved PL measurements. The steady-state model in eq 1 can be rewritten as

$$\frac{d\langle N(t)\rangle}{dt} = -\frac{\langle N(t)\rangle}{\tau_r} - C_{bx}\langle N(t)^2\rangle \quad (2)$$

and the resulting carrier recombination dynamics can then be extracted from the solution to the differential equation:

$$\langle N(t)\rangle = \frac{\langle N(0)\rangle e^{-t/\tau_r}}{1 + \tau_r\langle N(0)\rangle C_{bx}(1 - e^{-t/\tau_r})} \quad (3)$$

where $\langle N(t)\rangle$ is the exciton concentration as a function of time, $\langle N(0)\rangle$ is the initial exciton concentration, and τ_r and C_{bx} are the same values as in the steady-state model mentioned above.[23] In order to fit the full carrier dynamics to the recombination model, multiple decay spectra were measured at various initial exciton concentrations, as shown in Figure S3. The resulting spectra were

DOI: 10.1021/acsnano.7b02521
ACS Nano 2017, 11, 5179−5185

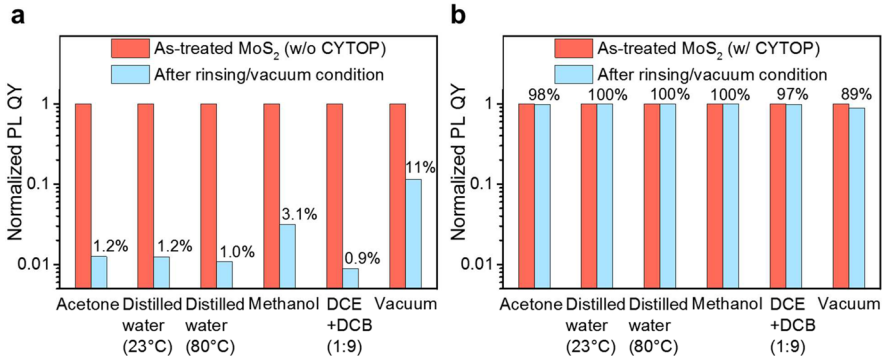

Figure 4. (a) PL QY of TFSI treated MoS_2 samples (a) not coated by CYTOP and (b) coated by 100 nm of CYTOP after various processing. Solvent exposure was conducted by immersing the sample in each solvent for 15 s. For vacuum conditions, MoS_2 sample was coated by 2 μm of secondary CYTOP layer after 100 nm of CYTOP and subsequent TFSI treatment.

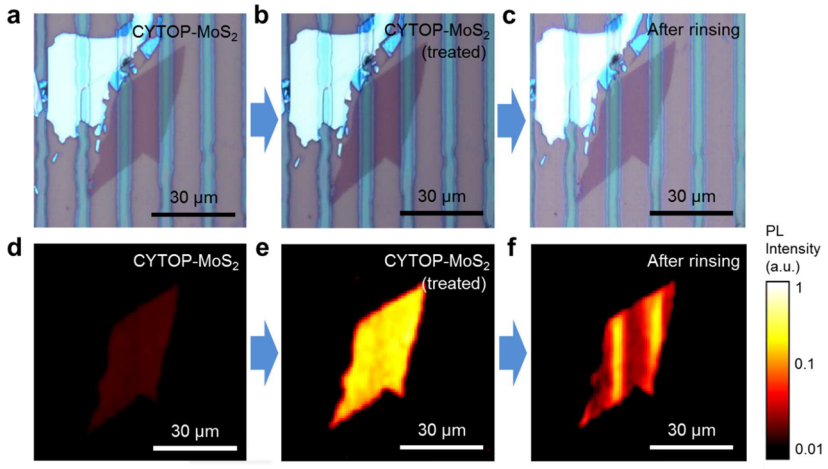

Figure 5. (a–c) Optical micrographs and (d–f) corresponding PL images of an as-prepared CYTOP-patterned MoS_2 monolayer, after treatment by TFSI, and after rinsing with water for 15 s; PL images are plotted on a common logarithmic scale.

then combined to form a single decay curve with over 5 orders of magnitude of dynamic range. Using the recombination parameters we extracted from the steady-state experiments, the time-resolved results can be fit to the dynamic model, which is given in eq 3. The radiative lifetime (τ_r) of the treated CYTOP-encapsulated MoS_2 was measured to be 15 ns, which is similar to what has been reported in our previous work without CYTOP.[23,24]

To investigate the mechanism of TFSI passivation of CYTOP-encapsulated MoS_2, QY was measured at a low pump intensity ($\sim 3 \times 10^{-3}$ W cm^{-2}) as a function of treatment time and CYTOP thickness, as shown in Figure 3a. Both the increases in QY with TFSI exposure time and with decreasing CYTOP thickness suggest a diffusional mechanism. We constructed a simple model for the process as follows. First, based on other studies which discussed the diffusion kinetics regarding TFSI or polymer film,[25−29] the diffusion of TFSI through CYTOP satisfies the criterion of Fickian diffusion. It is assumed that the swelling effect of the CYTOP film by the solvent is negligible, allowing the concentration of TFSI $c(x,t)$ to be described as

$$\frac{c(x,\,t) - c(x,\,0)}{c_s - c(x,\,0)} = 1 - \mathrm{erf}\left(\frac{x}{2\sqrt{Dt}}\right) \tag{4}$$

where x is the distance from the interface between the bulk solution and the surface of the CYTOP, t is diffusion time, D is the TFSI diffusion coefficient in CYTOP, and c_s is the TFSI concentration at the interface between the bulk solution and the surface of the CYTOP (x = 0). We used Fourier transform infrared (FTIR) spectroscopy to measure the TFSI diffusion into the CYTOP. Here, the samples were rinsed with 1,2-dichloroethane (DCE)/1,2-dichlorobenzene (DCB), which were solvents for TFSI solution, to remove residual TFSI molecules from the top surface. As shown in Figure 3b, absorption peaks associated with TFSI were observed after treatment and increased with increasing treatment time. While CYTOP contains a significant number of C−F bonds, the S−N−S and S═O peaks can directly be attributed to the diffused TFSI. As such, the enhanced peak intensities can be used to measure the concentration of diffused TFSI within the CYTOP layer. Figure 3c shows the time-dependent absorption A_t at 1325 ± 25 and 1140 ± 25 cm^{-1} for a 100 nm CYTOP layer normalized to the steady state values, A_{eq}, measured after 40 min of exposure. The diffusion coefficient measured from FTIR spectroscopy is 1.1×10^{-14} cm^2 s^{-1} and the dotted line is a fit to $c(x,t)$ integrated from 0 to L, which is described as[25,30]

$$\frac{A_t}{A_{eq}} = 1 - \frac{8}{\pi^2}\sum_{m=0}^{\infty}\frac{1}{(2m+1)^2}\exp\left(\frac{-D(2m+1)^2\pi^2 t}{L^2}\right) \tag{5}$$

We adapted a model used for describing surface passivation in hydrogenated silicon to relate the QY of the of MoS_2 monolayer to the concentration of TFSI at its surface $c(L,t)$:

DOI: 10.1021/acsnano.7b02521
ACS Nano 2017, 11, 5179−5185

$$QY \propto e^{-(N_d - K \times c(L,t) \times d)} \propto e^{K \times c(L,t)} \quad (6)$$

where N_d is total defect concentration, d is the thickness of monolayer, and K is introduced as a passivation constant, indicating the effectiveness of defect passivation by TFSI.[31−33] The solid lines in Figure 3a are obtained from solving eqs 4 and 6 with a diffusion coefficient of 1.2×10^{-14} cm^2 s^{-1}, which is a value nearly identical to that obtained from the FTIR measurement. The simple model is in excellent quantitative agreement with the experimental data, showing that the increase of QY over treatment time can be explained through diffusion of TFSI into the CYTOP layer.

We found that CYTOP encapsulation not only promotes a high yield and control of PL QY enhancement during treatment but also preserves the near-unity PL QY against external conditions. Figure 4a,b illustrates the stability of CYTOP-encapsulated MoS_2 monolayers after TFSI treatment, compared to treated samples without encapsulation. For TFSI treated MoS_2 without encapsulation, the PL QY is significantly degraded after processing with each solvent for 15 s or when the sample is exposed to low pressure (~10^{-5} Torr). Due to the high chemical resistance and hydrophobicity of CYTOP, we find that it is also able to act as a protective capping layer.[34−37] For vacuum measurement, to minimize the release of diffused TFSI by degassing of the fluoropolymer at low pressure, a secondary, thicker CYTOP (~2 μm) layer was additionally spin-coated after CYTOP encapsulation and subsequent TFSI treatment. Also, for the vacuum-processed sample, the Raman spectrum of CYTOP-encapsulated MoS_2 monolayer after treatment was measured to ensure that there is negligible strain, which may be caused by the volume change of CYTOP under vacuum condition (Figure S4). The PL QY of CYTOP-encapsulated WS_2 monolayer is also stable against post-rinsing processing and various external conditions.

Finally, we demonstrate that CYTOP encapsulant can be patterned, which provides a potential route toward the fabrication of practical devices. We develop a patterning method that consists of photolithography and lift-off of CYTOP. Figure 5 shows the PL images and corresponding optical micrographs of a MoS_2 monolayer with CYTOP patterns which were examined after treatment and after subsequent rinsing in water. After treatment, both exposed and CYTOP encapsulated portions of the monolayer showed high and uniform PL QY. When the treated MoS_2 monolayer with CYTOP patterns was rinsed with water, significant degradation of the PL in the unencapsulated regions was observed. However, as shown in Figure 5f, the part of the MoS_2 monolayer with CYTOP encapsulation retained high PL QY. This result indicates that our encapsulating layer, which is compatible with a general patterning process, can be stable during subsequent fabrication process and suitable for future device applications, preserving dramatically enhanced PL QY against external conditions.

CONCLUSION

In conclusion, we have demonstrated 2D TMDCs with near-unity PL QY and excellent stability through superacid treatment after encapsulation by an environment-resistive fluoropolymer. Based on the diffusion mechanism, TFSI is able to penetrate through CYTOP encapsulant and suppresses defect-mediated nonradiative recombination in the monolayer, resulting in near-unity PL QY in both MoS_2 and WS_2 at low injection levels. Our encapsulation and treatment strategy can facilitate emerging studies on the excitonic properties and the mechanism of defect passivation in 2D TMDCs due to the additional control during treatment. Furthermore, due to its ability to be directly patterned and its compatibility with general fabrication processes, this method can potentially be utilized for the fabrication of high-performance 2D optoelectronic devices.

METHODS

Sample Preparation and Encapsulation. Quartz was used as the substrate for all calibrated optical measurements. The substrates were cleaned in a piranha solution for 15 min and subsequently rinsed with acetone, isopropyl alcohol (IPA), and deionized (DI) water for 5 min. MoS_2 was mechanically exfoliated on quartz substrate from bulk crystals (SPI). Prior to spin-coating, samples were annealed in forming gas (5% H_2, 95% N_2) at 300 °C for 3 h. In order to obtain 100 nm thick CYTOP film, a CYTOP solution (CTL-809M, Asahi Glass Co.) was diluted in its solvent (CT-Solv.180, Asahi Glass Co.) to make a 3 wt % CYTOP solution and spin-coated at 500 rpm for 10 s, then at 4000 rpm for 30 s, followed by thermal annealing in a N_2 ambient, where the temperature was gradually increased from 30 to 200 °C over a span of 50 min.

Chemical Treatment. A procedure for superacid treatment used in this work was similar to the method described in the previous studies,[23,24] but with further optimization. Prior to solution preparation, all chemical bottles were first opened inside a N_2 atmosphere. Twenty mg of TFSI (Sigma-Aldrich) was dissolved in 10 mL of DCE (Sigma-Aldrich) to make a 2 mg/mL TFSI solution and further diluted with DCB (Sigma-Aldrich) to make a 0.2 mg/mL TFSI solution in a 1:9 mixture of DCE and DCB. For treatment, samples and solution were taken out from the glovebox, and then samples were immersed in the 0.2 mg/mL TFSI solution for 40 min under ambient air condition at room temperature. After the samples were removed from the solution, they were blow-dried with nitrogen without rinsing or annealing.

Optical Spectroscopy. The instruments and procedures used for calibrated steady-state and transient optical characterization utilized here were same as our previous study.[23] In brief, the 514.5 nm line of Ar^+ laser (Lexel 95) was used for excitation in steady-state PL and Raman measurements, and the power density was adjusted by neutral density filters. The power of incident laser beam was continuously monitored by a photodiode power meter (ThorLabs S120C); in order to accurately measure low laser powers, the power on the laser diode was approximately 100× higher than the power incident on the sample. A CCD detector (Andor iDus BEX2-DD) on a f = 340 mm spectrometer with a 150 g/mm grating was used for steady-state measurements. The CCD background was measured prior to the PL measurement and subtracted from the PL acquisition. The external sample PL efficiency was determined using the wavelength-dependent response and the collection efficiency of the instrument, which were estimated using previously described methods after the measurement. The absolute internal PL QY was extracted using the quantitative absorption data. Time-resolved measurements were performed using a 514 nm line selected from a supercontinuum laser (Fianium WhiteLase SC-400) using a double monochromator and subsequently detected using a single photon counting avalanche photodiode (IDQuantique) and analyzed using a time-correlated single photon counting module (Becker-Hickl GmbH). Raman measurements were measured in the backscattering geometry and using a triple spectrometer configured in subtractive mode with a 2400 g/mm grating in the final stage. For all measurements, the laser was focused on the sample using a 50× objective lens with a numerical aperture of 0.55. PL images were acquired on MoS_2 monolayers prepared by gold exfoliation[38] using a florescence microscopy setup and a 470 nm LED as the excitation source. IR absorption measurements were performed using an FTIR microscope (Nicolet, ThermoFisher). Prior to IR absorption measurements, the samples were rinsed with DCE/DCB to remove residual TFSI molecules on the sample surface.

Stability Characterization. Stability tests were performed on TFSI treated MoS_2 samples with and without CYTOP encapsulation. After PL QY measurement for as-treated samples, each sample was immersed in acetone, distilled water (80 °C), methanol, and DCE/DCB (1:9 in weight ratio) for 15 s, respectively. When the samples were removed

DOI: 10.1021/acsnano.7b02521
ACS Nano 2017, 11, 5179−5185

from solvents, they were blow-dried with nitrogen, and the QY was measured using the same procedure as was performed for as-treated samples. For vacuum measurement, after CYTOP encapsulation and subsequent TFSI treatment, a secondary, thicker CYTOP (~2 μm) layer was additionally spin-coated and annealed at 80 °C for 30 min in a N_2 ambient. PL QY measurements in the vacuum chamber were performed at a pressure <10^{-5} Torr.

Patterning Process. MoS_2 monolayers were prepared on a cleaned 260 nm SiO_2/Si substrate and spin-coated with a positive photoresist (S1818, Shipley) at 500 rpm for 5 s and then at 3000 rpm for 30 s, followed by baking at 115 °C for 60 s on a hot plate. After UV exposure at a constant intensity of 100 mJ/cm^2, the sample was developed with MF-26A (Microchem) for 1 min, rinsed with DI water, and blow-dried with nitrogen. A 3 wt % CYTOP solution was then spin-coated at 500 rpm for 10 s/4000 rpm for 30 s. The sample was heated on a hot plate at 80 °C for 2 min. To remove the photoresist and the CYTOP layer on the remaining photoresist, the lift-off was carried out by immersing the sample in warm acetone for 1 h. Finally, the sample was thermally annealed to postbake the CYTOP patterns using the same procedure described as above.

ASSOCIATED CONTENT

Supporting Information

The Supporting Information is available free of charge on the ACS Publications website at DOI: 10.1021/acsnano.7b02521.

Pump-power dependence of PL QY on a treated CYTOP-coated WS_2 monolayer (Figure S1); AFM measurements after various stages of sample processing (Figure S2); full time-resolved PL measurements with various initial exciton concentrations (Figure S3); Raman spectrum under vacuum condition (Figure S4) (PDF)

AUTHOR INFORMATION

Corresponding Author

*E-mail: ajavey@eecs.berkeley.edu.

ORCID

Der-Hsien Lien: 0000-0001-6774-2074
Joel W. Ager: 0000-0001-9334-9751
Ali Javey: 0000-0001-7214-7931

Author Contributions

‖These authors contributed equally to this work.

Notes

The authors declare no competing financial interest.

ACKNOWLEDGMENTS

This work was supported by the Electronic Materials Program funded by the Director, Office of Science, Office of Basic Energy Sciences, Materials Sciences and Engineering Division of the U.S. Department of Energy, under contract no. DE-AC02-05Ch11231.

REFERENCES

(1) Radisavljevic, B.; Radenovic, A.; Brivio, J.; Giacometti, V.; Kis, A. Single-Layer MoS_2 Transistors. *Nat. Nanotechnol.* **2011**, *6*, 147−150.

(2) Wang, Q. H.; Kalantar-Zadeh, K.; Kis, A.; Coleman, J. N.; Strano, M. S. Electronics and Optoelectronics of Two-Dimensional Transition Metal Dichalcogenides. *Nat. Nanotechnol.* **2012**, *7*, 699−712.

(3) Xu, M.; Liang, T.; Shi, M.; Chen, H. Graphene-Like Two-Dimensional Materials. *Chem. Rev.* **2013**, *113*, 3766−3798.

(4) Jariwala, D.; Sangwan, V. K.; Lauhon, L. J.; Marks, T. J.; Hersam, M. C. Emerging Device Applications for Semiconducting Two-Dimensional Transition Metal Dichalcogenides. *ACS Nano* **2014**, *8*, 1102−1120.

(5) Ionescu, A. M.; Riel, H. Tunnel Field-Effect Transistors as Energy-Efficient Electronic Switches. *Nature* **2011**, *479*, 329−337.

(6) Splendiani, A.; Sun, L.; Zhang, Y.; Li, T.; Kim, J.; Chim, C.-Y.; Galli, G.; Wang, F. Emerging Photoluminescence in Monolayer MoS_2. *Nano Lett.* **2010**, *10*, 1271−1275.

(7) Ruppert, C.; Aslan, O. B.; Heinz, T. F. Optical Properties and Band Gap of Single- and Few-Layer $MoTe_2$ Crystals. *Nano Lett.* **2014**, *14*, 6231−6236.

(8) Ramasubramaniam, A.; Naveh, D.; Towe, E. Tunable Band Gaps in Bilayer Transition-Metal Dichalcogenides. *Phys. Rev. B: Condens. Matter Mater. Phys.* **2011**, *84*, 205325.

(9) Desai, S. B.; Seol, G.; Kang, J. S.; Fang, H.; Battaglia, C.; Kapadia, R.; Ager, J. W.; Guo, J.; Javey, A. Strain-Induced Indirect to Direct Bandgap Transition in Multilayer WSe_2. *Nano Lett.* **2014**, *14*, 4592−4597.

(10) McCreary, A.; Ghosh, R.; Amani, M.; Wang, J.; Duerloo, K.-A. N.; Sharma, A.; Jarvis, K.; Reed, E. J.; Dongare, A. M.; Banerjee, S. K.; Terrones, M.; Namburu, R. R.; Dubey, M. Effects of Uniaxial and Biaxial Strain on Few-Layered Terrace Structures of MoS_2 Grown by Vapor Transport. *ACS Nano* **2016**, *10*, 3186−3197.

(11) Britnell, L.; Ribeiro, R. M.; Eckmann, A.; Jalil, R.; Belle, B. D.; Mishchenko, A.; Kim, Y.-J.; Gorbachev, R. V.; Georgiou, T.; Morozov, S. V.; Grigorenko, A. N.; Geim, A. K.; Casiraghi, C.; Castro Neto, A. H.; Novoselov, K. S. Strong Light-Matter Interactions in Heterostructures of Atomically Thin Films. *Science* **2013**, *340*, 1311−1314.

(12) Fang, H.; Battaglia, C.; Carraro, C.; Nemsak, S.; Ozdol, B.; Kang, J. S.; Bechtel, H. A.; Desai, S. B.; Kronast, F.; Unal, A. A.; Conti, G.; Conlon, C.; Palsson, G. K.; Martin, M. C.; Minor, A. M.; Fadley, C. S.; Yablonovitch, E.; Maboudian, R.; Javey, A. Strong Interlayer Coupling in van der Waals Heterostructures Built from Single-Layer Chalcogenides. *Proc. Natl. Acad. Sci. U. S. A.* **2014**, *111*, 6198−6202.

(13) Miller, O. D.; Yablonovitch, E.; Kurtz, S. R. Strong Internal and External Luminescence as Solar Cells Approach the Shockley−Queisser Limit. *IEEE J. Photovol.* **2012**, *2*, 303−311.

(14) Ye, Y.; Wong, Z. J.; Lu, X.; Ni, X.; Zhu, H.; Chen, X.; Wang, Y.; Zhang, X. Monolayer Excitonic Laser. *Nat. Photonics* **2015**, *9*, 733−737.

(15) Sundaram, R. S.; Engel, M.; Lombardo, A.; Krupke, R.; Ferrari, A. C.; Avouris, P.; Steiner, M. Electroluminescence in Single Layer MoS_2. *Nano Lett.* **2013**, *13*, 1416−1421.

(16) Zhao, W.; Ghorannevis, Z.; Chu, L.; Toh, M.; Kloc, C.; Tan, P.-H.; Eda, G. Evolution of Electronic Structure in Atomically Thin Sheets of WS_2 and WSe_2. *ACS Nano* **2013**, *7*, 791−797.

(17) Mak, K. F.; Lee, C.; Hone, J.; Shan, J.; Heinz, T. F. Atomically Thin MoS_2: A New Direct-Gap Semiconductor. *Phys. Rev. Lett.* **2010**, *105*, 136805.

(18) Yuan, L.; Huang, L. Exciton Dynamics and Annihilation in WS_2 2D Semiconductors. *Nanoscale* **2015**, *7*, 7402−7408.

(19) Wang, H.; Zhang, C.; Rana, F. Ultrafast Dynamics of Defect-Assisted Electron−Hole Recombination in Monolayer MoS_2. *Nano Lett.* **2015**, *15*, 339−345.

(20) Tongay, S.; Zhou, J.; Ataca, C.; Liu, J.; Kang, J. S.; Matthews, T. S.; You, L.; Li, J.; Grossman, J. C.; Wu, J. Broad-Range Modulation of Light Emission in Two-Dimensional Semiconductors by Molecular Physisorption Gating. *Nano Lett.* **2013**, *13*, 2831−2836.

(21) Mouri, S.; Miyauchi, Y.; Matsuda, K. Tunable Photoluminescence of Monolayer MoS_2 *via* Chemical Doping. *Nano Lett.* **2013**, *13*, 5944−5948.

(22) Peimyoo, N.; Yang, W.; Shang, J.; Shen, X.; Wang, Y.; Yu, T. Chemically Driven Tunable Light Emission of Charged and Neutral Excitons in Monolayer WS_2. *ACS Nano* **2014**, *8*, 11320−11329.

(23) Amani, M.; Lien, D.-H.; Kiriya, D.; Xiao, J.; Azcatl, A.; Noh, J.; Madhvapathy, S. R.; Addou, R.; Kc, S.; Dubey, M.; Cho, K.; Wallace, R. M.; Lee, S.-C.; He, J.-H.; Ager, J. W.; Zhang, X.; Yablonovitch, E.; Javey, A. Near-Unity Photoluminescence Quantum Yield in MoS_2. *Science* **2015**, *350*, 1065−1068.

(24) Amani, M.; Taheri, P.; Addou, R.; Ahn, G. H.; Kiriya, D.; Lien, D.-H.; Ager, J. W.; Wallace, R. M.; Javey, A. Recombination Kinetics and Effects of Superacid Treatment in Sulfur- and Selenium-Based Transition Metal Dichalcogenides. *Nano Lett.* **2016**, *16*, 2786−2791.

DOI: 10.1021/acsnano.7b02521
ACS Nano 2017, 11, 5179−5185

(25) Alfrey, T.; Gurnee, E. F.; Lloyd, W. G. Diffusion in Glassy Polymers. *J. Polym. Sci., Part C: Polym. Symp.* **1966**, *12*, 249−261.
(26) Crank, J. *The Mathematics of Diffusion*, 2nd ed.; Oxford University Press: Oxford, 1975.
(27) Masaro, L.; Zhu, X. X. Physical Models of Diffusion for Polymer Solutions, Gels and Solids. *Prog. Polym. Sci.* **1999**, *24*, 731−775.
(28) Bowyer, W. J.; Xu, W.; Demas, J. N. Determining Proton Diffusion in Polymer Films by Lifetimes of Luminescent Complexes Measured in the Frequency Domain. *Anal. Chem.* **2009**, *81*, 378−384.
(29) Wapner, K.; Grundmeier, G. Spatially Resolved Measurements of the Diffusion of Water in a Model Adhesive/Silicon Lap Joint Using FTIR-Transmission-Microscopy. *Int. J. Adhes. Adhes.* **2004**, *24*, 193−200.
(30) Musto, P.; Galizia, M.; La Manna, P.; Pannico, M.; Mensitieri, G. Diffusion and Molecular Interactions in a Methanol/Polyimide System Probed by Coupling Time-Resolved FTIR Spectroscopy with Gravimetric Measurements. *Front. Chem.* **2014**, *2*, 1−9.
(31) Street, R. A. Recombination in Amorphous Semiconductors. *Phys. Rev. B: Condens. Matter Mater. Phys.* **1978**, *17*, 3984−3995.
(32) Street, R. A.; Knights, J. C.; Biegelson, D. K. Luminescence Studies of Plasma-Deposited Hydrogenated Silicon. *Phys. Rev. B: Condens. Matter Mater. Phys.* **1978**, *18*, 1880−1891.
(33) Sidhu, L. S.; Kosteski, T.; Zukotynski, S.; Kherani, N. P.; Shmayda, W. T. Effect of Dangling-Bond Density on Luminescence in Tritiated Amorphous Silicon. *Appl. Phys. Lett.* **1999**, *74*, 3975−3977.
(34) Kalb, W. L.; Mathis, T.; Haas, S.; Stassen, A. F.; Batlogg, B. Organic Small Molecule Field-Effect Transistors with Cytop Gate Dielectric: Eliminating Gate Bias Stress Effects. *Appl. Phys. Lett.* **2007**, *90*, 092104.
(35) Walser, M. P.; Kalb, W. L.; Mathis, T.; Brenner, T. J.; Batlogg, B. Stable Complementary Inverters with Organic Field-Effect Transistors on Cytop Fluoropolymer Gate Dielectric. *Appl. Phys. Lett.* **2009**, *94*, 053303.
(36) Cheng, X.; Caironi, M.; Noh, Y.-Y.; Wang, J.; Newman, C.; Yan, H.; Facchetti, A.; Sirringhaus, H. Air Stable Cross-Linked Cytop Ultrathin Gate Dielectric for High Yield Low-Voltage Top-Gate Organic Field-Effect Transistors. *Chem. Mater.* **2010**, *22*, 1559−1566.
(37) Choi, S.-H.; Jang, J.-H.; Kim, J.-J.; Han, M.-K. Low-Temperature Organic (CYTOP) Passivation for Improvement of Electric Characteristics and Reliability in IGZO TFTs. *IEEE Electron Device Lett.* **2012**, *33*, 381−383.
(38) Desai, S. B.; Madhvapathy, S. R.; Amani, M.; Kiriya, D.; Hettick, M.; Tosun, M.; Zhou, Y.; Dubey, M.; Ager, J. W.; Chrzan, D.; Javey, A. Gold-Mediated Exfoliation of Ultralarge Optoelectronically-Perfect Monolayers. *Adv. Mater.* **2016**, *28*, 4053−4058.

DOI: 10.1021/acsnano.7b02521
ACS Nano 2017, 11, 5179−5185